Original Research Article

Journal of Tissue Engineering
Volume 15: 1–18

DOI: 10.1177/20417314241268912
journals.sagepub.com/home/tej
Sage

Vascularized characteristics and functional regeneration of three-dimensional cell reconstruction of oral mucosa equivalents based on vascular homeostasis phenotypic modification

Lijuan Shi[1,2], Yiwen Xu[1,2], Jingying Li[1,2], Li He[1,2], Kaiyu Li[1,2], Shigang Yin[3], Minhai Nie[1,2] and Xuqian Liu[1,2]

Abstract

Our prior research has effectively developed tissue-engineered vascularized oral mucosa equivalents (VOME); however, challenges such as low repeatability and stability, as well as the inability to accurately replicate the complexity of real blood vessels, were encountered. Therefore, this study aimed to screen the VOME and native oral mucosa vascular homeostasis phenotypes by tandem mass tag-tagged proteomics associated with laser capture microdissection and human angiogenesis antibody array technology. Then, lentiviruses were constructed and stably transfected with vascular endothelial-like cells (VELCs) to detect angiogenic capacity. HE, EdU Apollo tracer staining, immunofluorescence staining, scanning electron microscopy, biomechanical testing, and a small animal ultrasound imaging system were used to analyze the characteristics of vascularization homeostasis and monitor functional regeneration of the vascularized homeostatic phenotypic oral mucosal equivalents (VHPOME). The results showed that PGAM1, COL5A1, ANG, and RNH1 are potential specific angiogenesis phenotypes. High expression of PGAM1, COL5A1, and ANG and/or low expression of RNH1 can promote the angiogenesis of VOME. ANG/shRNH1 has the most significant tube-like structure-formation ability. The expression of PGAM1, COL5A1, and ANG in the VHPOME group was higher than that of the control group, and the expression of RNH1 was lower than that of the control group. COL5A1/ANG can significantly improve the mechanical properties. The blood flow signal was most significant in the ANG/shRNH1 group. PGAM1, COL5A1, ANG, shRNH1, PGAM1/ANG, COL5A1/ANG, PGAM1/shRNH1, PGAM1/shRNH1, COL5A1/shRNH1, and ANG/shRNH1 may be the targets for establishing vascularization homeostasis and functional regeneration of oral mucosal equivalent genes (groups), and ANG/shRNH1 has the most significant effect.

Keywords

Vascular endothelial-like cells, oral mucosal equivalent, vascularization homeostasis, laser capture microdissection, ANG-RNH1 system

Date received: 22 April 2024; accepted: 9 July 2024

[1]Department of Periodontics & Oral Mucosal Diseases, The Affiliated Stomatology Hospital of Southwest Medical University, Luzhou, Sichuan, China
[2]Oral & Maxillofacial Reconstruction and Regeneration of Luzhou Key Laboratory, Luzhou, Sichuan, China
[3]Laboratory of Neurological Diseases and Brain Function, The Affiliated Hospital of Southwest Medical University, Luzhou, Sichuan, China

Corresponding author:
Xuqian Liu, Department of Periodontics & Oral Mucosal Diseases, The Affiliated Stomatological Hospital of Southwest Medical University, Oral & Maxillofacial Reconstruction and Regeneration of Luzhou Key Laboratory, No. 10, Section 2, Yunfeng Road, Jiangyang District, Luzhou, Sichuan 646000, China.
Email: liuxuqianwork@163.com

Introduction

Oral and maxillofacial trauma, congenital anomalies, and malignant tumors often lead to large areas of oral mucosal soft tissue defects. At present, skin grafts or flaps are mainly used for repair, but their sources are limited,[1] and mucosal or skin transplantation may cause new wounds and donor site complications. In recent years, tissue engineering methods based on cells and scaffolds have been deeply studied, which indicates that tissue engineering oral mucosa equivalents have potential clinical application value and provide a new solution for the repair and reconstruction of oral and maxillofacial soft tissue defects.[2]

Organoids can simulate the complexity of human tissues, but they still lack stable and functional vascular systems. The vasculature is a conduit for the transport of nutrients, oxygen, and metabolites.[3] The diameter of the equivalent oral mucosa constructed in vitro is more than 200–400 μm, and the cells inside it will be difficult to obtain nutrition and oxygen support through infiltration after implantation in vivo. If internal blood circulation cannot be established, the wound will atrophy without perfusion of the vascular system, and it will be difficult to fully restore the appearance and function of the damaged mucosa.[4] Therefore, the construction of mature and functional vasculature is a difficulty in the construction of tissue engineering organoids. Since the oral mucosa is rich in blood vessels, it is of great significance to enhance angiogenesis before implantation and continuous vascularization after implantation to ensure that the tissue-engineered oral mucosa equivalents can be revascularized and have sufficient blood supply.

Based on our previous studies,[5,6] 3D cell reconstruction has successfully constructed tissue-engineered vascularized oral mucosa equivalents (VOME), which reveals that the key to realizing the survival of oral mucosa equivalents is the formation of oral mucosa organoids with vascular networks. However, previous studies still lack standardization and procedure, and have low repeatability and stability, which can only be used as a model for short-term research. Due to the lack of a dynamic perfusion process in the vascularization of the oral mucosal equivalent, it is difficult to fully simulate real blood vessels. In addition, the size and density of the equivalent vessel-like structures in the oral mucosa are quite different from those in vivo. Therefore, how to achieve repeatable, stable, and continuous vascularization of oral mucosal equivalents to form a programmed functional perfusion vascular system, that is, establishing a vascular homeostasis and maintaining the survival ability of the oral mucosal equivalents is still an urgent problem to be solved.

Therefore, based on the above questions, we aimed to explore the differential phenotypes of vascularization homeostasis of three-dimensional cell reconstruction oral mucosa equivalents. Then construct the vascularized steady-state phenotyped modified vascular endothelial-like cells (VELCs) loaded with acellular vascular matrix (ACVM)-0.25% human-like collagen I (HLC-I) modified composite matrix, and the characteristics of vascularization homeostasis and functional regeneration were monitored.

Materials and methods

Animals and acquisition of rabbit abdominal aorta

SPF female nude mice (3–4 weeks, 15 g) were purchased from Beijing Huafukang Biotechnology Co., Ltd. (No. SCXK (Beijing) 2019-0008). The abdominal aorta of the New Zealand White rabbits (SCXK (Chongqing) 2017-0010) was used for scaffold preparation. Animal experiments have been approved by the Laboratory Animal Ethics Committee of Southwest Medical University (No. 201909-1).

Acquisition of gingival tissues

Gingival tissues were collected from healthy adolescents aged 18–24 who underwent flap resection for the extraction of mandibular impacted third molars at the Affiliated Stomatological Hospital of Southwest Medical University. The experiment has passed the ethical review of the Affiliated Stomatological Hospital of Southwest Medical University (No. 20190828001). Informed consent was obtained from patients and their guardians.

Construction of vascularized oral mucosa equivalents (VOME)

Based on our previous study,[6] human gingival epithelial tissue and connective tissue were primarily cultured. The third passage of human gingival epithelial cells (HGECs) and human gingival fibroblasts (HGFs) in good growth condition were selected to prepare cell slides. The cells were identified using immunocytofluorescence and immunohistochemistry. Gingival mesenchymal stem cells (GMSCs) were induced with 8 ng/mL vascular endothelial growth factor 165 ($VEGF_{165}$) for 35 days to differentiate into VELCs.

HGECs and VELCs in good growth condition were cultured in a culture medium containing 10 μM EdU, respectively. After 24 h, labeled HGECs and VELCs were fixed with 4% paraformaldehyde for 30 min, incubated with a 2 mg/mL glycine solution for 5 min, and washed with PBS for 5 min, respectively. Apollo® staining reaction solution 488 stained HGECs, Apollo® staining reaction solution 567 stained VELCs, and DAPI stained HGFs.

Our previous studies have confirmed that ACVM-0.25% HLC-I biological scaffolds have favorable biological characteristics,[5,6] and its preparation methods are as follows: New Zealand White rabbits were anesthetized through the intravenous administration of 6 mL/kg of a 0.7% pentobarbital sodium solution injected into the ear margin. Subsequently, the abdominal aorta was excised, and the rabbits underwent euthanasia by receiving an intravenous injection of 6 mL/kg of a 5% pentobarbital sodium solution at the ear margin. The abdominal aorta of the rabbits was then rinsed with saline and trimmed to a length of 2 cm before being immersed in PBS containing 1% benzabroman for 1 h at ambient temperature. Following a PBS rinse, the blood vessels were placed in a 0.1% pancreatic enzyme solution and incubated in a 5% CO_2 environment at 37℃ for 6 h. Subsequently, the blood vessels were washed with PBS and incubated in a 1% TritonX-100 PBS solution for an additional 72 h at room temperature. The ACVM scaffolds were then washed with PBS, and both 1 cm-long sheet ACVM scaffolds and 2 mm-thick ring ACVM scaffolds were prepared. These ACVM scaffolds underwent treatment with an acrylic acid solution, followed by a PBS wash, and were then transferred to a 5 mg/mL water-soluble carbodiimide solution for immersion for 1 h at 4℃. After a PBS rinse, the scaffolds were combined with a 0.25% HLC-I solution at room temperature for 5 h to create the ACVM-0.25% HLC-I bioscaffolds (Figure 1(a)).

DAPI-labeled HGFs and EdU Apollo 567-labeled VELCs (1×10^6/mL) were combined with Matrigel in a ratio of 4:1. After mixing, they were seeded on the ACVM-0.25% HLC-I scaffolds and placed in an incubation box for co-culture for 1 week to obtain HGFs-ACVM-0.25% HLC-I and VELCs-ACVM-0.25% HLC-I. Ten microliter of matrix glue was dropped on the surface of HGFs-ACVM-0.25% HLC-I and placed in the incubation box for 30 min. After the matrix glue became gelatinized, the VELCs-ACVM-0.25% HLC-I was planted on the surface of the HGFs-ACVM-0.25% HLC-I and co-cultured in the incubation box for 1 week to form HGFs-VELCs-ACVM-0.25% HLC-I. HGECs labeled with EdU Apollo 488 in the logarithmic growth phase were selected, digested with trypsin, and the cell concentration was adjusted to 1×10^6/mL, mixed with Matrigel in a 4:1 ratio, and then planted on HGFs-VELCs-ACVM-0.25% HLC-I. They were placed in an incubation box and co-cultured for 1 week to obtain the HGECs-HGFs-VELCs-ACVM-0.25% HLC-I complex (Figure 1(b)).

Ten nude mice, aged 4–5 weeks, were anesthetized by intraperitoneal injection with 0.5 mL/100 g of a 0.5% sodium pentobarbital solution. A 1.0×1.0 cm full-thickness incision was made on the left back, and the HGECs-HGFs-VELCs-ACVM-0.25% HLC-I complex was implanted. After 14 days, the subcutaneous polyurethane film was removed, the wound surface was coated with biological glue, and EdU Apollo 488-labeled HGECs were implanted on the surface of the biological glue. Following the surgery, all the nude mice woke up and were returned to the SPF animal laboratory. After 14 days of care, the nude mice were euthanized by intraperitoneal injection with 0.5 mL/100 g of a 5% sodium pentobarbital solution, and tissue samples were collected at the implantation site.

Observation of VOME

The constructed oral mucosa equivalent tissues were paraffin-embedded and sectioned. After being deparaffinized in water, the sections were stained with HE and EdU. Normal oral mucosa and VOME were embedded in optimum cutting temperature (OCT) embedding medium, placed at −20℃ to solidify the tissue block, prepared into 12 μm thin sections, and sliced onto PEN membrane slides. HE staining was performed after the OCT embedding medium on the sections was completely dissolved. Laser capture microdissection (LCM) targets the capture of neovascular-like structures in VOME.

Proteomics tandem mass tags (TMT) analysis

The vessel-like structures of normal oral mucosa and VOME were obtained by LCM and protein concentration was measured using the BCA method. The protein was precipitated with acetone, redissolved, reduced, and alkylated, followed by enzymatic digestion, labeling with TMT, removal of SDC, peptide desalting, and high-pH fractionation. Nano-scale liquid chromatography–tandem mass spectrometry (NanoLC-MS/MS) detection, library identification, and protein quantitative data analysis.

Human angiogenesis antibody microarray

Human angiogenesis antibody microarray analysis was conducted using the Human Angiogenesis Array Kit (No. ARY007, R&D, USA) on proteins from normal oral mucosal vascular structures and vascular-like structures of VOME obtained by LCM. The film was immersed in a 4-well dish containing 2 mL of Array Buffer 7 and incubated for 1 h. Subsequently, 0.5 mL of Array Buffer 4 and 1 mL of sample protein were added to the tube, and Array Buffer 5 was used to adjust the final volume to 1.5 mL. Then, 15 μL of the reconstituted assay antibody mixture was added. Array Buffer 7 was blotted out, and the sample/antibody mixture in the tube was incubated overnight at 2–8℃. Following membrane washing with 1× Washing buffer, the membranes were exposed to secondary antibodies for 30 min. A prepared chemical reagent mixture was carefully added to the membrane and incubated for 1 min before being placed under X-ray film for visualization.

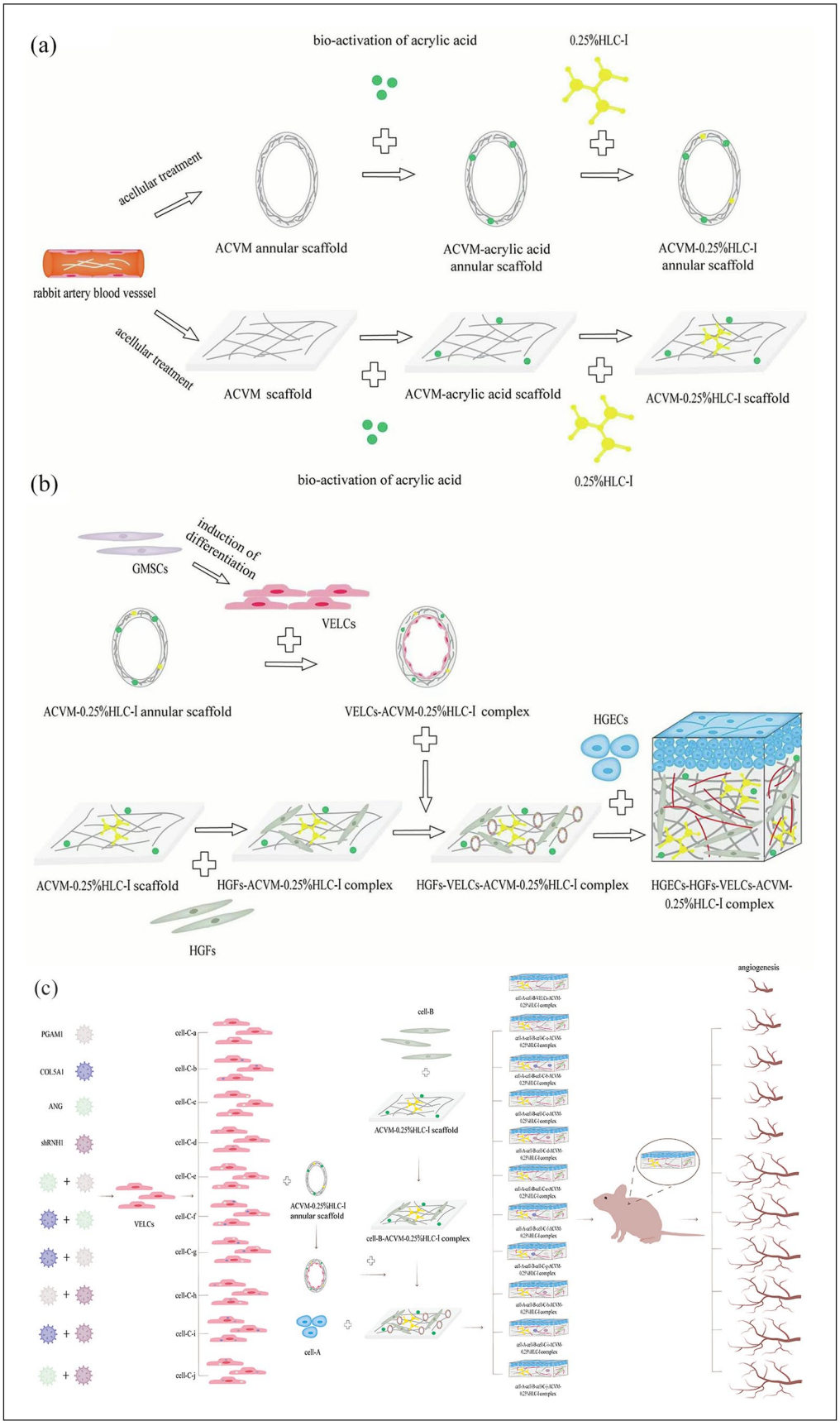

Figure 1. (a) The construction diagram of ACVM-0.25% HLC-I scaffold, (b) the construction diagram of HGECs-HGFs-VELCs-ACVM-0.25% HLC-I complex, (c) the diagram of dynamic reinforcement experimental model of bioreactor in vivo.

Western blot analysis

Proteins were extracted from both the VOME and normal oral mucosa tissue, followed by determination of protein concentration. Subsequently, SDS-PAGE gel electrophoresis was conducted. PVDF membranes were activated with methanol and utilized for protein transfer, followed by blocking with 5% skimmed milk powder for 1.5 h. The membranes were then exposed to primary antibody solutions (GAPDH, 1:4000, AB0037, Abways, Shanghai, China; ANG, 1:1000, E-7133, Aidtech, Beijing, China; PGAM1, 1:2000, bs-5006R, Bioss, Beijing, China; RNH1, 1:2000, bs-7518R, Bioss, Beijing, China; CD54, 1:1500, bs-0608R, Bioss, Beijing, China; CD105, 1:1000, bs-34063R, Bioss, Beijing, China; CD51, 1:2000, bs-2250R, Bioss, Beijing, China; vWF, 1:2000, 10973-T24, Sino Biological, Beijing, China; CD34, 1:2000, BA0532, Boster, Wuhan, China; Tie-2, 1:1000, bs-1300R, Bioss, Beijing, China; CD31, 1:2000, BA1346, Boster, Wuhan, China; COL5A1, 1:1000, bs-0552R, Bioss, Beijing, China; VEGFR1, 1:1000, 2904, SAB, United States; VEGFR2, 1:1000, AF4726, Affinity, USA) and incubated overnight at 4℃. Then, transfer to secondary antibody working solution 1:10000 and incubate at room temperature for 1 h. The images were collected after development on the computer.

Protein enrichment analysis

Gene enrichment analysis of proteins in VOME that interact with angiotensin (ANG) using the GO database (https://geneontology.org/).

Co-immunoprecipitation validation of RNH1 and ANG interactions in oral mucosal equivalents

The ribonuclease inhibitor 1 (RNH1) antibody was bound to Protein A+G Agarose Gel. The oral mucosa equivalent protein extract was added to Protein A+G Agarose Gel conjugated with the RNH1 antibody or Normal Rabbit IgG antibody for immunoprecipitation. A western blot was performed after eluting the precipitate with SDS-PAGE loading buffer.

Construction of PGAM1, COL5A1, ANG and shRNH1 lentivirus

Phosphoglycerate mutase 1 (PGAM1), collagen type 5 alpha1 (COL5A1), ANG, and depleted of RNH1 (shRNH1) lentivirus empty vectors were designed. The coding sequence of PGAM1 was retrieved from the National Center for Biotechnology Information (NCBI). Based on the sequence, the primer sequences for PGAM1, COL5A1, and ANG were synthesized. The target gene fragments were amplified by PCR, and the linearized expression vectors were prepared. The target genes were then constructed into the linearized expression vectors, transformed into recipient cells, colonies were identified by PCR, positive clones were sent for sequencing and plasmid extraction, lentiviral packaging, and titer detection. For shRNH1, the designed primers annealed to form a double-stranded fragment with a sticky end. Subsequently, the target gene and interference fragment were constructed into the prepared expression vector, transformed into competent cells, identified by colony PCR, and positive clones were sequenced and plasmids extracted.

Transfection and stability screening

Prepared VELCs (5×10^5/mL) were seeded in 6-well plates, with 2 mL per well, and cultured in a 37℃, 5% CO_2 incubator for 24 h. PGAM1, COL5A1, ANG, shRNH1 lentivirus, and their corresponding empty vector lentivirus were transfected into VELCs at a multiplicity of infection (MOI) of 20 and virus titer. Twelve hours after transfection, the medium containing lentivirus was replaced with fresh medium. At 48 h after transfection, the corresponding antibiotics were added to each well to screen the stable transformants, and the stable VELCs strains were obtained approximately 1 week after transfection.

Tube formation ability test

The pre-cooled Matrigel matrix gel was added to a 48-well plate on an ice surface in a sterile environment, at 100 μL per well. After gentle shaking, the 48-well plate was placed in a 37℃ incubator for 30 min to allow the matrix gel to solidify. Cell suspension was prepared when the bottom of the bottle was about 80% filled with VELCs and transfected VELCs. 5×10^5 cells/mL were collected and seeded in a 48-well plate coated with adhesive, 100 μL per well. The untransfected (control), PGAM1, COL5A1, ANG, shRNH1, PGAM1/ANG, COL5A1/ANG, PGAM1/COL5A1, PGAM1/shRNH1, COL5A1/shRNH1, and ANG/shRNH1 groups were each set up with three replicates. The 48-well plates were then placed in an incubator, removed after 24 h, and photographed under an inverted microscope for documentation.

Construction of the vascularized homeostatic phenotypic oral mucosal equivalents (VHPOME)

EdU Apollo 488 was used to label the third passage HGECs in good growth condition (cell-A). The third passage HGFs (cell-B) were labeled with DAPI staining solution. The VELCs were named cell-C, EdU Apollo 567 labeled cell-C, over-expressing PGAM1 transfected cell-C (Cell-C-a), over-expressing COL5A1 transfected

cell-C (Cell-C-b), over-expressing ANG transfected cell-C (Cell-C-c), silencing RNH1 transfected cell-C (Cell-C-d), and over-expressing PGAM1 + ANG co-transfected cell-C (Cell-C-e), over-expressing COL5A1 + ANG co-transfected cell-C (Cell-C-f), over-expressing PGAM1+COL5A1 co-transfected cell-C (Cell-C-g), PGAM1 overexpression and RNH1 silencing were co-transfected into cell-C (Cell-C-h), COL5A1 overexpression and RNH1 silencing were co-transfected into cell-C (Cell-C-i), ANG overexpression and RNH1 silencing were co-transfected into cell-C (Cell-C-j).

Based on our previous research, cell-A-cell-B-cell-C-ACVM-0.25% HLC-I, cell-A-cell-B-cell-C-a-ACVM-0.25% HLC-I,cell-A-cell-B-cell-C-b-ACVM-0.25%HLC-I,cell-A-cell-B-cell-C-c-ACVM-0.25% HLC-I, cell-A-cell-B-cell-C-d-ACVM-0.25%HLC-I,cell-A-cell-B-cell-C-e-ACVM-0.25% HLC-I, cell-A-cell-B-cell-C-f-ACVM-0.25% HLC-I, cell-A-cell-B-cell-C-g-ACVM-0.25% HLC-I, cell-A-cell-B-cell-C-h-ACVM-0.25% HLC-I, cell-A-cell-B-cell-C-i-ACVM-0.25% HLC-I, and cell-A-cell-B-cell-C-j-ACVM-0.25% HLC-I were constructed. The nude mice were subcutaneously implanted with the above scaffold complex and euthanized by intraperitoneal injection with 0.5 mL/100g 5% sodium pentobarbital solution 4 weeks later, and tissue samples were collected at the implanted site (Figure 1(c)).

Observation of VHPOME

The three-dimensional reconstructed equivalent tissue sections of the VHPOME group were deparaffinized in water, followed by HE staining and EdU Apollo tracer staining. For immunofluorescence staining, the cells were incubated with 3% H_2O_2 for 10 min, blocked with 5% BSA for 30 min, incubated with primary antibodies (labeled with PGAM1, COL5A1, ANG, and RNH1) at 4℃ overnight, incubated with secondary antibodies goat anti-rabbit TRITC and goat anti-mouse FITC for 1 h, and counterstained with DAPI for 15 min. The slides were sealed with 5% glycerin and observed under an inverted microscope.

The samples were washed, fixed with 3% glutaraldehyde, postfixed with 1% osmic acid for 1 h, and dehydrated. Subsequently, the sample was affixed to the sample holder using conductive glue, which was then inserted into an ion sputtering instrument for spray plating. A scanning electron microscope was employed to examine the vessel-like structure and distribution of the samples, and images were captured.

Tissue biomechanical properties test

The samples were kept moist by placing them in saline. The INSTRON 5965 universal mechanical testing instrument was used to measure the stress-time and stress-strain changes of the samples. Each sample was secured to the ends of the mechanical tester using a needle holder, and the tensile speed was set to 10 mm/min. The experiment concluded upon sample breakage, and the stress and strain data at each time point were noted and recorded.

Monitoring the blood flow signals of VHPOME

Nude mice were placed in an anesthesia induction box, and oxygen was adjusted to 1 L/min while isoflurane was set at 4%–5%. Following general anesthesia, the mice were positioned with the anesthesia mask covering their nose and mouth, and the maintenance dose of isoflurane was adjusted to 1%–2%. A coupling agent was applied to the metal electrodes of the mouse plate, and 3M transparent adhesive was used to secure the limbs of the nude mice to the four metal electrodes. The coupling agent was also applied to the implantation site on the left back. Using gray scale and color Doppler modes, the MX400 probe was positioned vertically at a 90° angle to the implantation site, and the probe was slowly adjusted until a clear image of the blood vessels was obtained.

Statistical analysis

The measurement data were expressed as mean ± standard deviation. The t-test was used for comparison between two groups, and one-way analysis of variance was used for comparison among multiple groups. $p < 0.05$ was considered statistically significant.

Results

Construction of VOME

The morphology of HGECs was clear, with cubical cells growing in cobblestone-like clumps, featuring round or oval nuclei and abundant cytoplasm. HGFs were well-defined, with cells displaying a typical long spindle shape, round or oval nuclei, and abundant cytoplasm. $VEGF_{165}$ induced GMSCs to differentiate into VELCs, which exhibited polygonal or cuboidal shapes with oval nuclei, resembling VECs (Figure 2(a)).

In the HGECs-labeled group, over 90% of the cells were labeled with EdU Apollo 488, and both the nucleus and cytoplasm exhibited green fluorescence. In the HGFs-labeled group, nearly all cells were labeled with DAPI, resulting in blue fluorescence in the nuclei. In the VECLs-labeled group, over 80% of the cells were labeled with EdU Apollo 567, displaying red fluorescence in both the nucleus and cytoplasm (Figure 2(b)).

HGECs-HGFs-VELCs-ACVM-0.25% HLC-I complex was implanted subcutaneously on the left back of nude mice. The suture fell off after 1 week, and the wound healed in approximately 2 weeks without obvious scar tissue formation (Figure 2(c)).

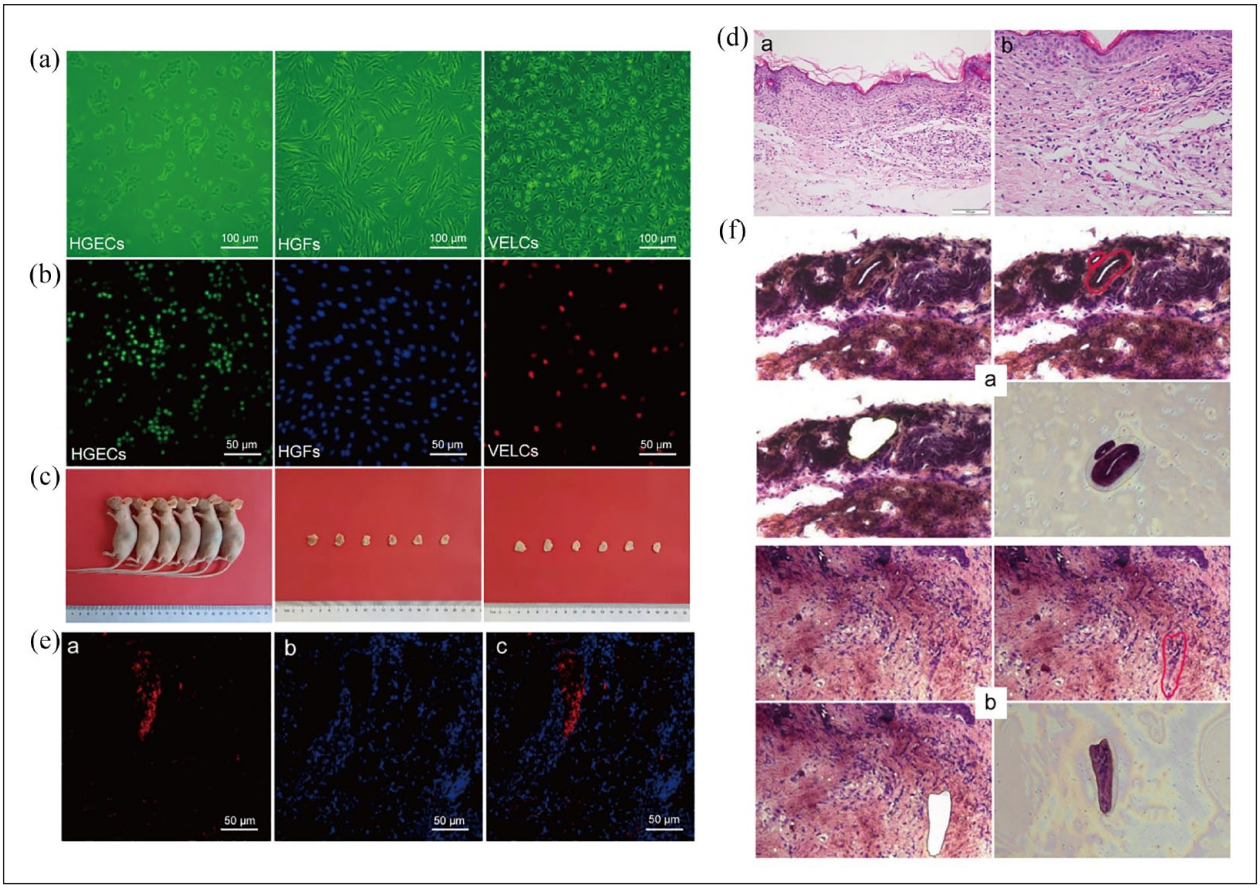

Figure 2. Construction and observation of the VOME: (a) cell culture (inverted microscope, ×100), (b) in vitro tracing of seed cells (inverted microscope, ×200), (c) in vivo dynamic enhancement experiments in bioreactors, (d) HE staining of VOME, (e) tracer observation of in vivo (EdU, ×200): (e-a) the vessel-like structure showed red fluorescence expression, (e-b) the lamina propria like structure showed blue fluorescence, (e-c) the neovascular-like structures formed by VELCs were distributed within the lamina propria like structures formed by HGFs, (f) LCM targeted capture of vascular-like structures (HE, ×200): (f-a) LCM targets vessel-like structures in VOME, (f-b) LCM targets vascular structures in normal oral mucosa.

Observation of VOME

HE showed that the VOME had structures similar to those of normal oral mucosa (Figure 2(d)). EdU Apollo 567-labeled VELCs exhibited red fluorescence expression and formed a vessel-like structure with a clear vascular lumen and a continuous closed wall. DAPI-labeled HGFs were expressed in blue fluorescence and distributed around the vessel-like structures, forming lamina propria-like structures (Figure 2(e)).

HE staining combined with LCM technology was used to target the vascular structure in the VOME and the vascular structure of normal oral mucosa. The results indicated that the morphology was similar (Figure 2(f)). The neovascular-like structure in the VOME exhibited a thick wall, a continuous closed oblong circle, and a thick lumen. Red blood cells were dispersed in the lumen, distributed within a lamina propria-like structure. In contrast, the wall of the capillary structure in native oral mucosa tissue was thinner than that in the VOME, and it appeared irregular and flat. The vascular lumen was smaller, with blood cells present in the lumen, distributed within the lamina propria structure beneath the epithelial tissue.

Proteomics analysis

SDS-PAGE combined with Coomassie Brilliant Blue staining was utilized to assess protein integrity. In this experiment, the protein samples exhibited clear bands and a uniform molecular weight distribution (Figure 3(a-a)). Each component of LC-MS quantitative proteomics was detected separately by the machine, demonstrating high repeatability and chromatographic stability (Figure 3(a-b)).

A total of 5406 proteins (groups) and 31,147 polypeptides were identified in this experiment. The distribution of protein peptide identification numbers is shown in Figure 3(b-a). The molecular weight distribution of the proteins is displayed in Figure 3(b-b). The peptide length distribution

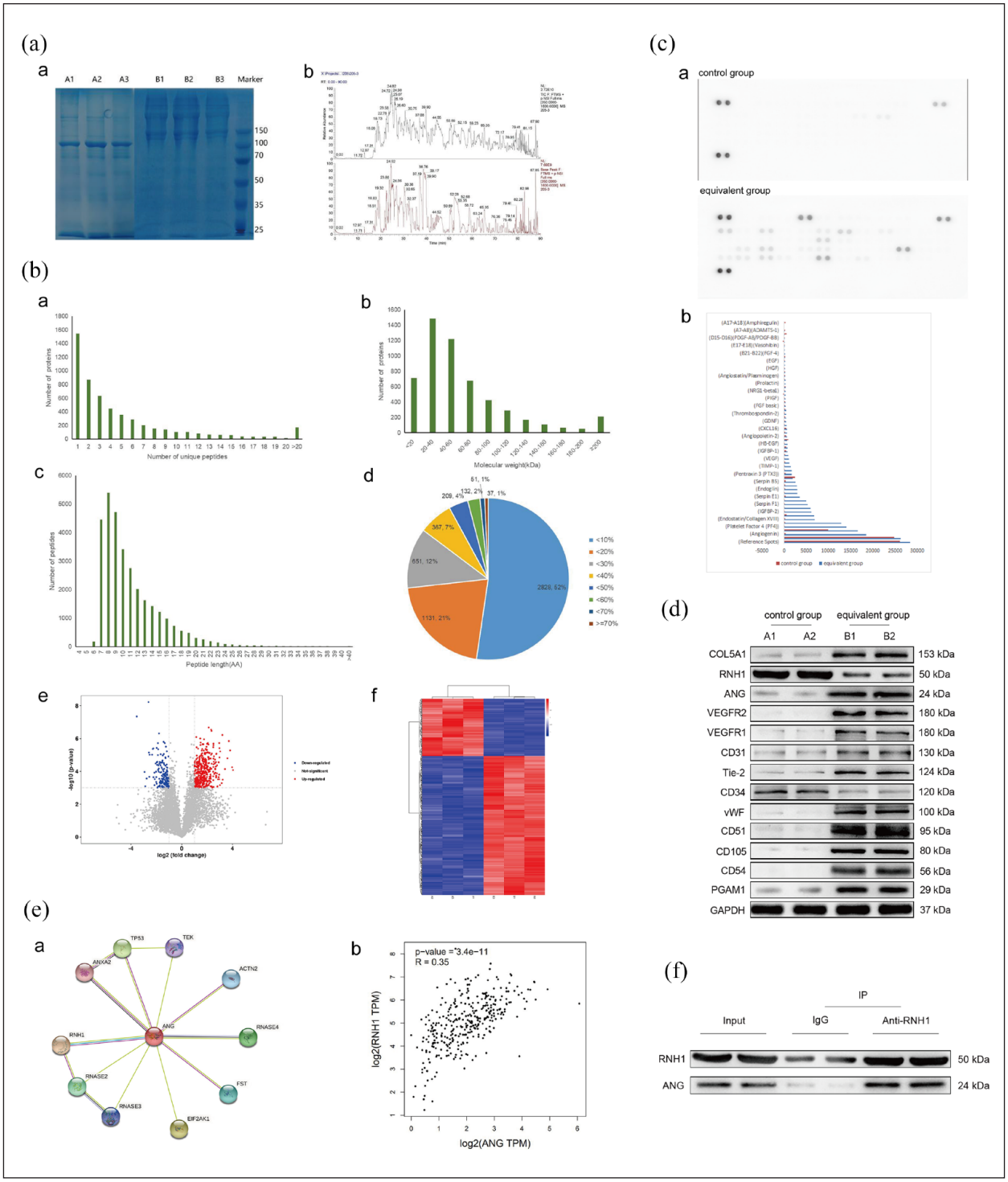

Figure 3. Proteomics analysis of the VOME: (a) results of protein quality control: (a-a) SDSPAGE+Coomassie brilliant blue staining, (a-b) TIC&BPC protein analysis, (b) protein analysis: (b-a) distribution of identified protein peptides, (b-b) protein molecular weight distribution, (b-c) peptide length distribution, (b-d) coverage distribution of protein identified peptides, (b-e) volcano plot of DEPs, (b-f) heat map of DEPs, (c) result of human angiogenesis array: (c-a) gray scale image of human angiogenesis antibody array results, (c-b) gray value comparison bar graph of human angiogenesis antibody chip, (d) the western blot results, (e) protein interaction network and correlation result between ANG and RNH1, (f) co-immunoprecipitation result.

is shown in Figure 3(b-c). The distribution of protein identification peptide coverage is shown in Figure 3(b-d). A total of 548 differentially expressed proteins (DEPs) were identified in the in VOME group compared with the native oral mucosa group, including 388 up-regulated proteins and 160 down-regulated proteins. Among them, the

Table 1. Tube forming properties of each group.

Groups (mean ± SD)	Number of tubes	Number of branching points	Total branching length (μm)	Total tubule length (μm)
Control	95.00 ± 45.21[a]	1498.67 ± 377.11[a]	37,114.00 ± 7598.44[a]	39,360.00 ± 6627.72[a]
PGAM1	247.33 ± 44.00[a]	2966.00 ± 251.40[a,b]	64,516.33 ± 7808.80[a–c]	66,471.67 ± 7460.52[a–c]
COL5A1	248.33 ± 41.04[a]	2321.33 ± 147.96[a]	48,108.67 ± 1481.40[a]	49,168.00 ± 617.51[a]
ANG	340.00 ± 90.51[a,b]	2927.33 ± 474.05[a,b]	53,252.67 ± 3899.40[a,b,d]	54,432.00 ± 3147.00[a,b,d]
shRNH1	324.33 ± 43.41[a,b]	3254.67 ± 354.01[a,b]	66,557.33 ± 2802.31[a–c]	68,726.00 ± 3154.31[a–c]
PGAM1/ANG	330.33 ± 96.01[a,b]	3368.33 ± 597.83[a,b]	64,854.67 ± 9201.76[a–c]	68,133.33 ± 9345.34[a–c]
COL5A1/ANG	374.00 ± 37.59[a,b]	3693.33 ± 283.03[b,c]	70,569.67 ± 5177.22[a–c]	72,898.67 ± 4986.88[a–c]
PGAM1/COL5A1	267.67 ± 73.38[a]	2690.67 ± 464.28[a,b]	51,215.67 ± 4340.59[a,d,e]	54,055.67 ± 5445.50[a,d,e]
PGAM1/shRNH1	267.67 ± 14.50[a]	3104.00 ± 137.16[a,b]	63,871.00 ± 657.44[a–c]	67,011.67 ± 450.78[a–c]
COL5A1/shRNH1	326.33 ± 113.56[a,b]	3304.00 ± 688.07[a,b]	67,184.33 ± 9731.05[a–c]	69,774.67 ± 9182.36[a–c]
ANG/shRNH1	576.33 ± 108.30[b]	4804.00 ± 681.70[b]	90,515.00 ± 6368.40[b,c]	91,748.67 ± 5923.38[b,c]

[a]Decreased compared with ANG/shRNH1 group ($p < 0.05$).
[b]Increased compared with control group ($p < 0.05$).
[c]Increased compared with COL5A1 group ($p < 0.05$).
[d]Decreased compared with COL5A1/ANG group ($p < 0.05$).
[e]Decreased compared with COL5A1/shRNH1 group ($p < 0.05$).

significantly up-regulated DEPs with higher abundance were COL5A1 and PGAM1, while the significantly down-regulated DEPs with higher abundance were RNH1, clathrin heavy chain 1 (CLTC), spectrin alpha chain erythrocytic 1 (SPTA1), ubiquitin-activating enzyme 1 (UBA1), Spectrin beta I (SPTB), and ankyrin 1 (ANK1). Figure 3(b-e) and 3(b-f) represents the volcano plot and heat map of differential proteins between the native oral mucosa group and VOME group, respectively.

Human angiogenesis antibody microarray analysis revealed that the angiogenic factors expressed in the VOME group are significantly different from those in the native oral mucosa group. The quantity and content of these factors are notably higher in the VOME group compared to the native oral mucosa group. Notably, ANG is the most significantly expressed angiogenic factor (Figure 3(c)).

Based on the results of TMT and human angiogenesis antibody microarray, we selected COL5A1, PGAM1, RNH1, and ANG for further study. The aforementioned proteins and VECs-specific markers CD31, CD34, CD51, CD54, CD105, Tie-2, vWF, VEGFR1, and VEGFR2 were detected by western blot. The results indicated higher expression levels of CD31, CD51, CD54, CD105, Tie-2, vWF, VEGFR1, VEGFR2, ANG, PGAM1, and COL5A1 in the VOME group, while CD34 and RNH1 levels were lower compared to the native oral mucosa group (Figure 3(d)).

As illustrated in protein-protein interactions (PPI), the proteins most strongly correlated with ANG were RNH1, recombinant ribonuclease A4 (RNASE4), and recombinant annexin A2 (ANXA2). The correlation between RNH1 and ANG is statistically significant, showing a positive correlation (Figure 3(e)). Additionally, co-immunoprecipitation results revealed the presence of ANG protein in the oral mucosa equivalent when anti-RNH1 was present (Figure 3(f)), indicating the binding between RNH1 and ANG.

Lentivirus transfection

PGAM1 overexpression, COL5A1 overexpression, ANG overexpression, and RNH1 silencing lentiviruses were successfully constructed (Supplemental Table 1). Compared with the control group, the relative mRNA expression levels of PGAM1, COL5A1, and ANG were higher in the overexpression (OE) group, while those of shRNH1 and shRNH1 Y24638 were lower. There were no significant differences between the empty vector group (NC) group and the untransfected (control) group (Supplemental Figure 1).

Tube forming ability test

Under an inverted microscope, the cells in each group formed tubule-like structures with different diameters and continuous lumen (Figure 4). The number of tubes were significantly increased in the ANG, shRNH1, PGAM1/ANG, COL5A1/ANG, COL5A1/shRNH1, and ANG/shRNH1 groups compared with the control group ($p < 0.05$). Meanwhile, the ANG/shRNH1 group was significantly increased compared with other groups ($p < 0.05$).

The number of branching points increased in the PGAM1, ANG, shRNH1, PGAM1/ANG, COL5A1/ANG, PGAM1/COL5A1, PGAM1/shRNH1, COL5A1/shRNH1, and ANG/shRNH1 groups compared to the control group; and in the COL5A1/ANG group compared to the COL5A1 group. The ANG/shRNH1 group had an increased number of branching points compared to the control, PGAM1, COL5A1, ANG, shRNH1, PGAM1/ANG, PGAM1/

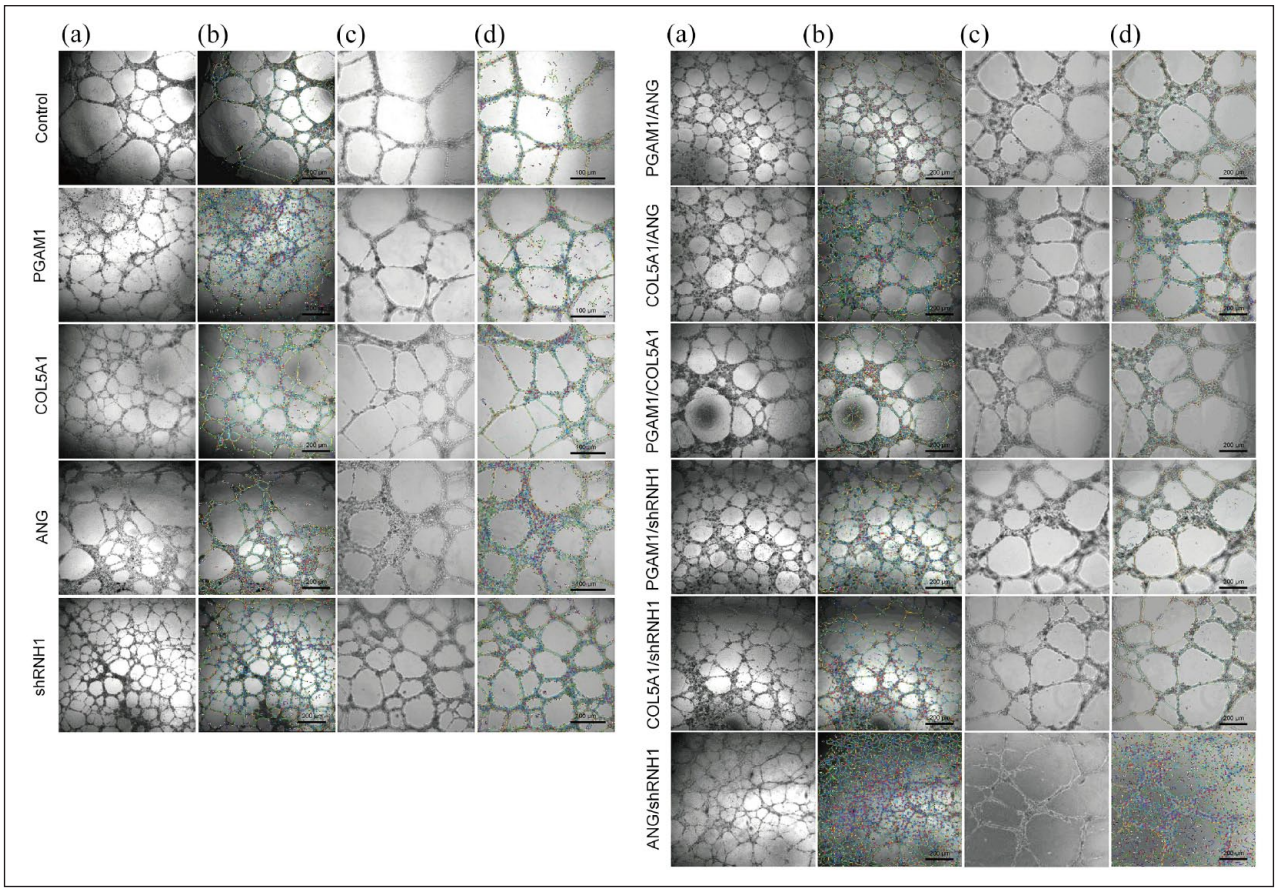

Figure 4. Tube formation: (a) VELCs and transfected VELCs were cultured in Matrigel for 24 h to form tubular structures (inverted microscope, ×40), (b) image J software was used to mark the tubular structures formed in each group (inverted microscope, ×40), (c) VELCs and transfected VELCs were cultured in matrigel for 24 h to form tubular structures (inverted microscope, ×100), (d) image J software marked the tubular structures formed in each group (inverted microscope, ×100).

COL5A1, PGAM1/shRNH1, and COL5A1/shRNH1 groups, and the difference was statistically significant ($p < 0.05$).

For the total branching length and total tubule length, PGAM1, ANG, shRNH1, PGAM1/ANG, COL5A1/ANG, PGAM1/shRNH1, COL5A1/shRNH1, ANG/shRNH1 groups increased compared to the control group; PGAM1, shRNH1, PGAM1/ANG, COL5A1/ANG, PGAM1/shRNH1, COL5A1/shRNH1, and ANG/shRNH1 groups increased compared to the COL5A1 group; the COL5A1/ANG group increased compared to the ANG, PGAM1/COL5A1 group; the COL5A1/shRNH1 group increased compared to the PGAM1/COL5A1 group; the ANG/shRNH1 group increased compared to the control, PGAM1, COL5A1, ANG, shRNH1, PGAM1/ANG, COL5A1/ANG, PGAM1/COL5A1, PGAM1/shRNH1, COL5A1/shRNH1 groups ($p < 0.05$) (Table 1).

Observation of the VHPOME

In vitro tracer labeling of seed cells showed that in HGECs-labeled group, more than 90% of the cells were labeled with EdU Apollo 488, and the nucleus and cytoplasm showed green fluorescence expression. In the HGFs-labeled group, almost all the cells were labeled with DAPI, and the nuclei showed blue fluorescence. In the untransfected and transfected-labeled groups, more than 80% of the cells were labeled with EdU Apollo 567, and the nucleus and cytoplasm showed red fluorescence expression (Figure 5(a)). The cell scaffold complex was implanted subcutaneously in nude mice, and the wounds were basically healed around 2 weeks, with no obvious scar tissue formation. After 4 weeks, tissue samples were taken, and the results are shown in Figure 5(b).

HE staining showed that there were a large number of seed cells in ACVM-0.25% HLC-I scaffolds. The oral mucosal equivalent tissue in each group formed a vessel-like structure with scattered red blood cells in the lumen (Figure 5(c)). Tissue structures similar to normal oral mucosa were formed in the bioreactor (i.e. nude mice models). VELCs labeled with EdU Apollo 567 were expressed in red fluorescence and formed a vessel-like structure with clear vascular lumen and continuous closed wall. DAPI-labeled HGFs were expressed in blue fluorescence and

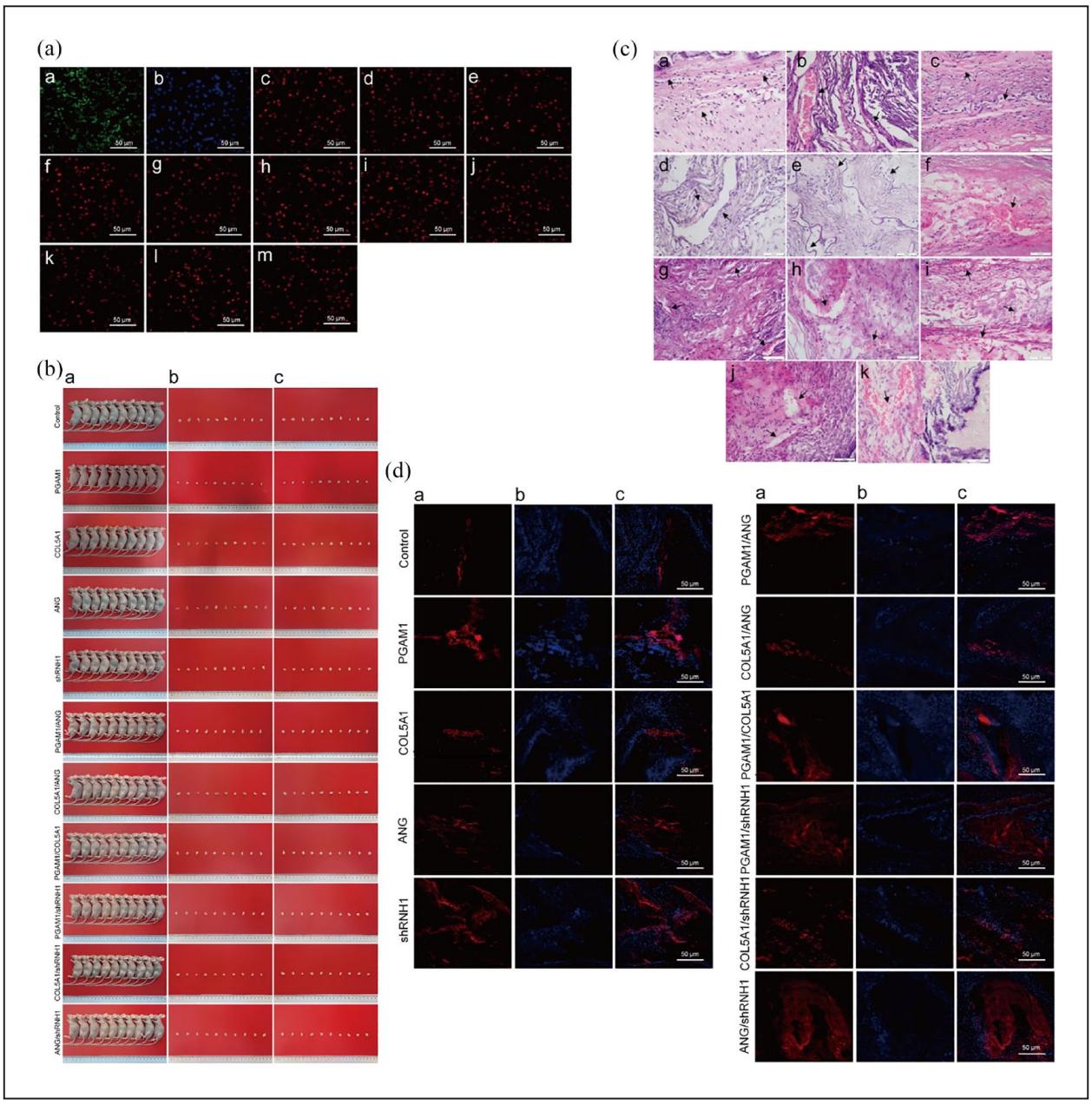

Figure 5. Observation of OMEVHP: (a) tracer observation of seed cell (inverted microscope, ×200): (a-a) EdU Apollo 488 labeled cell-A, (a-b) DAPI labeled cell-B, (a-c)—(a-m) are EdU567 Apollo labeled cell-C, Cell-C-a, Cell-C-b, Cell-C-c, Cell-C-d, Cell-C-e, Cell-C-f, Cell-C-g, Cell-C-h, Cell-C-i, and Cell-C-j, respectively, (b) dynamic reinforcement experiment in animal models bioreactor: (b-a) The complex was implanted subcutaneously on the left back of nude mice, and the tissue was harvested at 4 weeks after operation, (b-b) positive view of oral mucosal equivalent tissue, (b-c) negative view of oral mucosal equivalent tissue, (c) HE staining (HE, ×400): (c-a)—(c-k) were control group, PGAM1, COL5A1, ANG, shRNH1, PGAM1/ANG, COL5A1/ANG, PGAM1/COL5A1, PGAM1/shRNH1, COL5A1/shRNH1, and ANG/shRNH1, respectively. Arrows indicate vessel-like lumen-like structures, (d) tracer observation of in vivo (EdU, ×200): (d-a) the vessel-like structure showed red fluorescence expression, (d-b) the lamina propria like structure showed blue fluorescence, (d-c) the neovascular-like structures formed by VELCs were distributed within the lamina propria like structures formed by HGFs.

distributed around the vessel-like structures, forming lamina propria like structures (Figure 5(d)).

Immunohistochemical fluorescence staining of PGAM1, COL5A1, ANG, and RNH1 was performed on the OMEVHP and control oral mucosa equivalents, respectively. In the OMEVHP group, PGAM1, COL5A1, and ANG were functionally expressed in the neovascular-like structures of the oral mucosa equivalent, while RNH1 was not expressed. The transfected VELCs formed a continuous closed neovascular-like structure on the complex.

The vascular lumen was large, the vascular wall was thick, and the irregular flat circle was distributed in the lamina propria like structure formed by blue fluorescent labeled HGFs. In the control group, PGAM1, COL5A1, and ANG were also expressed in the neovascular-like structure of the oral mucosa equivalent, but the fluorescence expression was weaker than that of the OMEVHP group, and RNH1 was not significantly expressed. The vascular lumen of the neovascular-like structure formed by VELCs on the complex was smaller in diameter compared to the OMEVHP group. Vascular endothelial tip cells were present in the vascular lumen of the equivalent neovascular-like structures in the oral mucosa of each group except the shRNH1 group (Figure 6(a)). SEM showed that the ultrastructure of the oral mucosal equivalents in each group was vessel-like, with irregular lumen shape and occasional interruption of wall continuity. The oral mucosal equivalents of ANG, COL5A1/ANG, and ANG/shRNH1 groups showed their vessel-like structures anastomose with the blood vessels of the bioreactor to form a vascular network (Figures 6(b) and 7).

Biomechanical properties testing

The peak of tensile stress was 0.11 ± 0.01 MPa at 13.81 ± 5.85 s in the control group. PGAM1 group reached 0.12 ± 0.02 MPa at 12.74 ± 3.58 s; COL5A1 group reached 0.11 ± 0.02 MPa at 12.55 ± 3.40 s; ANG group reached 0.12 ± 0.03 MPa at 13.81 ± 2.96 s; shRNH1 group reached 0.12 ± 0.01 MPa at 13.96 ± 3.24 s; PGAM1/ANG group reached 0.13 ± 0.02 MPa at 12.63 ± 1.16 s; COL5A1/ANG group reached 0.13 ± 0.02 MPa at 24.09 ± 3.66 s; PGAM1/COL5A1 group reached 0.14 ± 0.02 MPa at 10.39 ± 2.85 s; PGAM1 /shRNH1 group reached 0.12 ± 0.01 MPa at 13.57 ± 1.41 s; COL5A1/shRNH1 group reached 0.12 ± 0.02 MPa at 15.87 ± 3.48 s; The ANG/shRNH1 group reached 0.13 ± 0.02 MPa at 14.19 ± 1.85 s. According to the stress-strain curve, the tensile strain corresponding to the peak tensile stress is as follows. The control, PGAM1, COL5A1, ANG, shRNH1, PGAM1/ANG, COL5A1/ANG, PGAM1/COL5A1, PGAM1/shRNH1, COL5A1/shRNH1, and ANG/shRNH1 groups were $22.26 \pm 9.57\%$, $21.19 \pm 6.57\%$, $21.92 \pm 4.56\%$, $25.00 \pm 5.84\%$, $30.74 \pm 4.88\%$, $20.72 \pm 1.80\%$, $39.85 \pm 6.07\%$, $17.14 \pm 4.09\%$, $22.51 \pm 2.37\%$, $26.11 \pm 5.81\%$, and $23.23 \pm 2.88\%$, respectively. Table 2 showed the biomechanical properties of each group.

Small animal ultrasound

The implantation site of the complex was dynamically monitored by a high-resolution small animal ultrasound system, and the gray scale mode was located to the vessel-like structure of the oral mucosa equivalent of each group. The red signal represents the blood flow toward the probe, and the blue signal represents the blood flow away from the probe. This indicated that there were multiple blood vessels in different directions in the equivalent, and the bioreactor established a good blood circulation. The blood flow signal of the OMEVHP group was more significant than that of the control group. The blood flow signal of ANG/shRNH1 group was the most significant (Figure 8).

Discussion

Despite significant progress in VOME research, lack of vascularization remains a major limitation.[7] Vascularization is very important for oxygen penetration, nutrient supply, and metabolite transport,[3] and only with the participation of the vascular system can oral mucosal equivalents continue to proliferate, differentiate, and mature. Previous studies have produced a pre-vascularized buccal mucosa model by co-cultivating HGECs and HGFs, and human dermal microvascular endothelial cells obtained from juvenile foreskin, on a collagen matrix (a commercial collagen matrix with porosity ranging from 5 μm to 300 nm) scaffold.[8] The selection of the scaffold material is an important step in the development of the VOME, which should be sufficiently biocompatible and biostable. Our previous study showed that compared to acellular dermal matrix (ADM), small intestinal submucosa (SIS) and Bio-Gide scaffolds, the ACVM-0.25% HLC-I scaffold was revealed to exhibit the best cell proliferation and good cell architecture, which has better biological characterization.[5] Angiogenesis is a complex process in which VECs connect to each other to form a new vascular network structure, which is one of the key links in the process of angiogenesis. Studies have found[9] that the presence of a large number of VECs is conducive to the rapid formation of blood vessels. Matrigel can be polymerized to form a three-dimensional structure with biological activity that mimics the composition, structure, and function of cell basement membrane in the human body, and is conducive to cell culture and differentiation in vitro.[10] The VOME obtained by implanting HGECs, HGFs, and VELCs on ACVM-0.25% HLC-I scaffolds using matrigel has good biocompatibility and biological strength.[11]

Pham et al.[12] detected sustained high expression of both cytokines after a few days by culturing cells carrying the genes for vascular endothelial growth factor and platelet-derived growth factor in vitro in a composite culture with scaffold material. Then they implanted the complex in vivo and observed that the number of new blood vessels in the new tissue was significantly higher than that in the control group. The subsequent study by Heller et al.[8] showed that the formation of microcapillaries was found to be significantly influenced by levels of angiogenic factors, with a greater reliance on VEGF and IL-8 levels. However, each study used different biomaterials, cell culture conditions, and preparation techniques, and there is a lack of

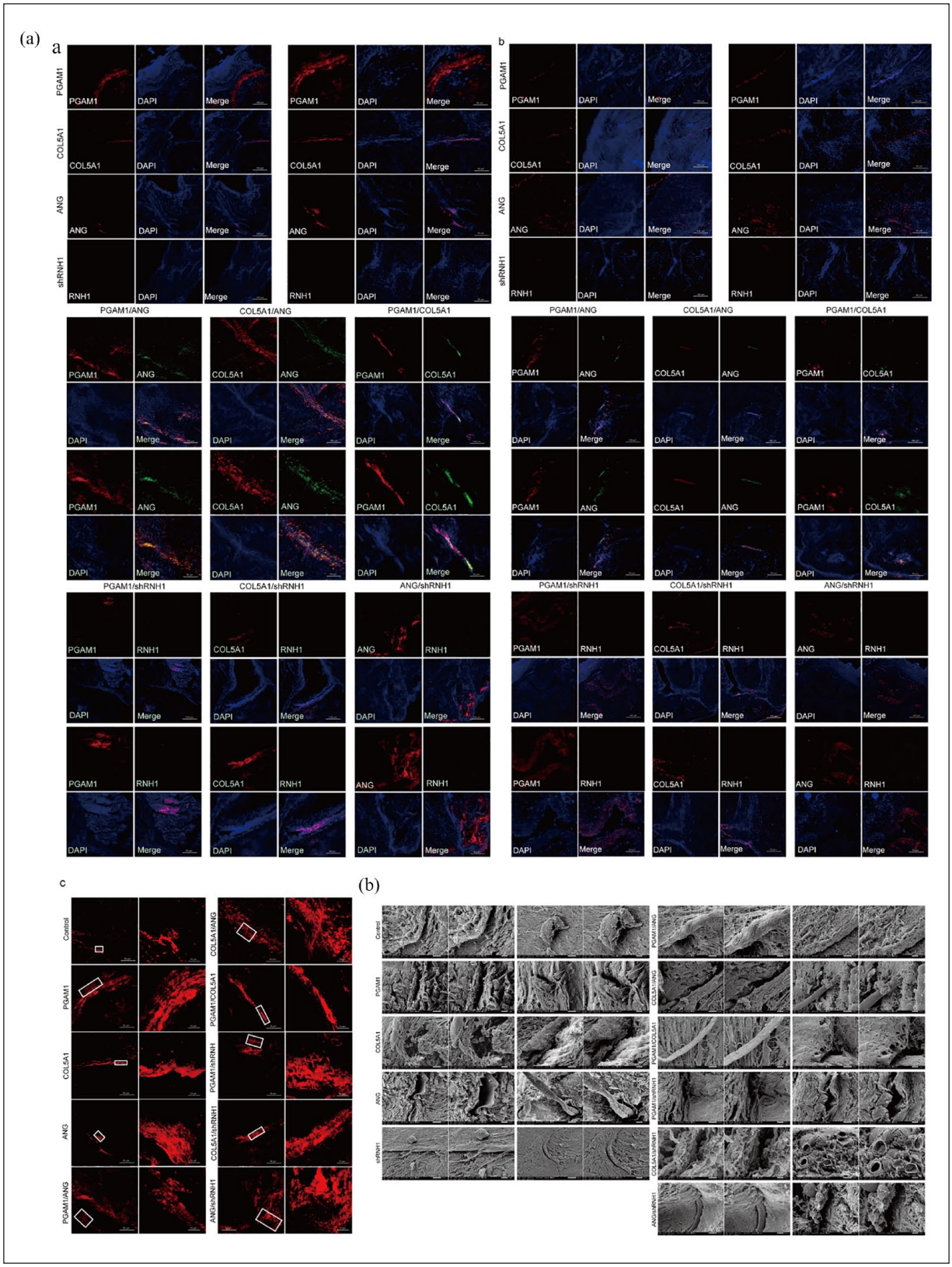

Figure 6. Observation of OMEVHP: (a) the immunofluorescent staining: (a-a) immunofluorescence staining of PGAM1, COL5A1, ANG, shRNH1 PGAM1/ANG, COL5A1/ANG, PGAM1/COL5A1, PGAM1/shRNH1, COL5A1/shRNH1, ANG/shRNH1 in oral mucosa; (a-b) immunofluorescence staining in VOME, (a-c) immunofluorescence staining observation of endothelial tip cells, (b) the vascular-like ultrastructure in each group was observed by SEM.

Table 2. Biomechanical properties of each group.

Group (mean ± SD)	Elastic modulus (MPa)	Maximum force value (N)	Tensile displacement at maximum value (mm)	Tensile stress at maximum value (MPa)	Tensile strain at maximum value (%)	Time at maximum value (s)
Control	0.79 ± 0.08	0.50 ± 0.12	2.23 ± 0.97	0.11 ± 0.01	22.26 ± 9.57	13.81 ± 5.85
PGAM1	0.78 ± 0.18	0.92 ± 0.03	2.08 ± 0.59[a]	0.12 ± 0.02	21.19 ± 6.57[a]	12.74 ± 3.58[a]
COL5A1	0.77 ± 0.09	0.93 ± 0.25	2.09 ± 0.65[a]	0.11 ± 0.02	21.92 ± 4.56[a]	12.55 ± 3.40[a]
ANG	0.84 ± 0.49	1.19 ± 0.53	2.46 ± 0.53[a]	0.12 ± 0.03	25.00 ± 5.84[a]	13.81 ± 2.96[a]
shRNH1	0.70 ± 0.03	0.85 ± 0.30	3.09 ± 0.49	0.12 ± 0.01	30.74 ± 4.88	18.96 ± 3.24
PGAM1/ANG	0.91 ± 0.29	1.43 ± 0.40	2.07 ± 0.18[a]	0.13 ± 0.02	20.72 ± 1.80[a]	12.63 ± 1.15[a]
COL5A1/ANG	0.59 ± 0.12	2.09 ± 0.85[b]	3.99 ± 0.61[b]	0.15 ± 0.02	39.85 ± 6.07[b]	24.09 ± 3.66[b]
PGAM1/COL5A1	1.07 ± 0.32	1.94 ± 1.03[b]	1.72 ± 0.41[a]	0.14 ± 0.02	17.14 ± 4.09[a]	10.39 ± 2.85[a]
PGAM1/shRNH1	0.80 ± 0.03	1.68 ± 0.30	2.26 ± 0.24[a]	0.12 ± 0.02	22.51 ± 2.37[a]	13.57 ± 1.41[a]
COL5A1/shRNH1	0.86 ± 0.30	1.57 ± 0.88	2.62 ± 0.58	0.12 ± 0.02	26.11 ± 5.81[a]	15.87 ± 3.48
ANG/shRNH1	1.12 ± 0.10	1.35 ± 0.39	2.33 ± 0.29[a]	0.13 ± 0.02	23.23 ± 2.88[a]	14.19 ± 1.85[a]

[a]Decreased compared with COL5A1/ANG group ($p < 0.05$).
[b]Increased compared with control group ($p < 0.05$).

available standard vascularization protocols.[7] To further explore the angiogenic factors of VOME, this study performed mass spectrometry and chip-targeted analysis of neovascularization-like structures of VOME and vascular structures in native oral mucosa tissue by LCM[13] combined with TMT and human angiogenesis antibody microarray. The results showed that PGAM1, COL5A1, ANG, and RNH1 are potential specific functional angiogenesis phenotypes with high abundance. PGAM1 is a key metabolic enzyme involved in the glycolytic pathway.[14] Glycolysis was found to be the predominant mode of energy metabolism in VECs, which can drive angiogenesis. Katrien DB et al.[15] prevented VECs from functioning properly by blocking the glycolytic process, which prevented angiogenesis. COL5A1 can maintain vascular tone and elasticity, which favors the growth of VECs and the adhesion of smooth muscle cells, and can maintain the mechanical properties of the vessel wall.[16] RNH1, an inhibitor of ribonuclease,[17] also binds tightly to vascular growth factors,[18] which can inhibit neovascularization. ANG is a potent inducer of vascular growth. It can regulate other angiogenic factors (e.g. VEGF, FGF, and EGF)[19] and promotes the proliferation of VECs,[20] which in turn induces neovascularization. ANG was found to phosphorylate Tie-2 after specific binding to the receptor Tie-2 on the cell membrane of VECs, affecting vascular permeability through activation of downstream pathways such as AKT and ERK, promoting angiogenesis, and maintaining the stability of the intravascular environment.[21] The roles of PGAM1, COL5A1, ANG, and RNH1 in angiogenesis were shown in supplemental Figure 2.

Western blot results showed that CD31 and CD34 were expressed in both VOME and natural oral mucosa. CD31 and CD34 are widespread vascular endothelial cell markers,[22–24] which are expressed in both native and neoplastic vascular endothelial cells,[25,26] and therefore do not reflect whether the vascular-like structures in the VOME originate from neovascularization. However, the expression levels of CD51, CD54, Tie-2, VEGFR1, VEGFR2, vWF, and CD105 were highly expressed in in vascularized oral mucosa equivalents, which were significantly different from natural oral mucosal tissues. It has been shown that they are expressed in pro-angiogenesis,[27–29] and regeneration of vascular injury repair,[30,31] which further confirms that VOME is consistent with the immunological profile of natural vascular neovascularization. The expression of PGAM1, COL5A1, and ANG was up-regulated in the neovasculature of VOME, whereas the expression of RNH1 was down-regulated, which was consistent with the results of TMT and human angiogenic antibody microarray analyses, suggesting that increased PGAM1, COL5A1, ANG, and/or decreased RNH1 may promote vascularization of oral mucosal equivalents. Protein interaction analysis showed that ANG was most closely related to RNH1 in the VOME. In order to further explore the vasogenesis mechanism of VOME, we investigated the interaction of the ANG-RNH1 system by co-immunoprecipitation. The results suggested that the ANG-RNH1 system may have an important role in establishing vascularization homeostasis.

The problems of insufficient sources and low culture efficiency of seed cells in the process of vascularization can be remedied by modifying cells by gene transfection.[32] To ensure that the tissue engineered oral mucosa equivalents can be revascularized and have sufficient blood supply, it is of great significance to enhance angiogenesis before implantation. Therefore, the angiogenic ability of lentivirus-modified VELCs with a vascularization homeostasis phenotype was investigated using the tube formation ability assay. The results showed that ANG, shRNH1, PGAM1/ANG, COL5A1/ANG, COL5A1/shRNH1, and ANG/shRNH1 could promote the tube formation ability of

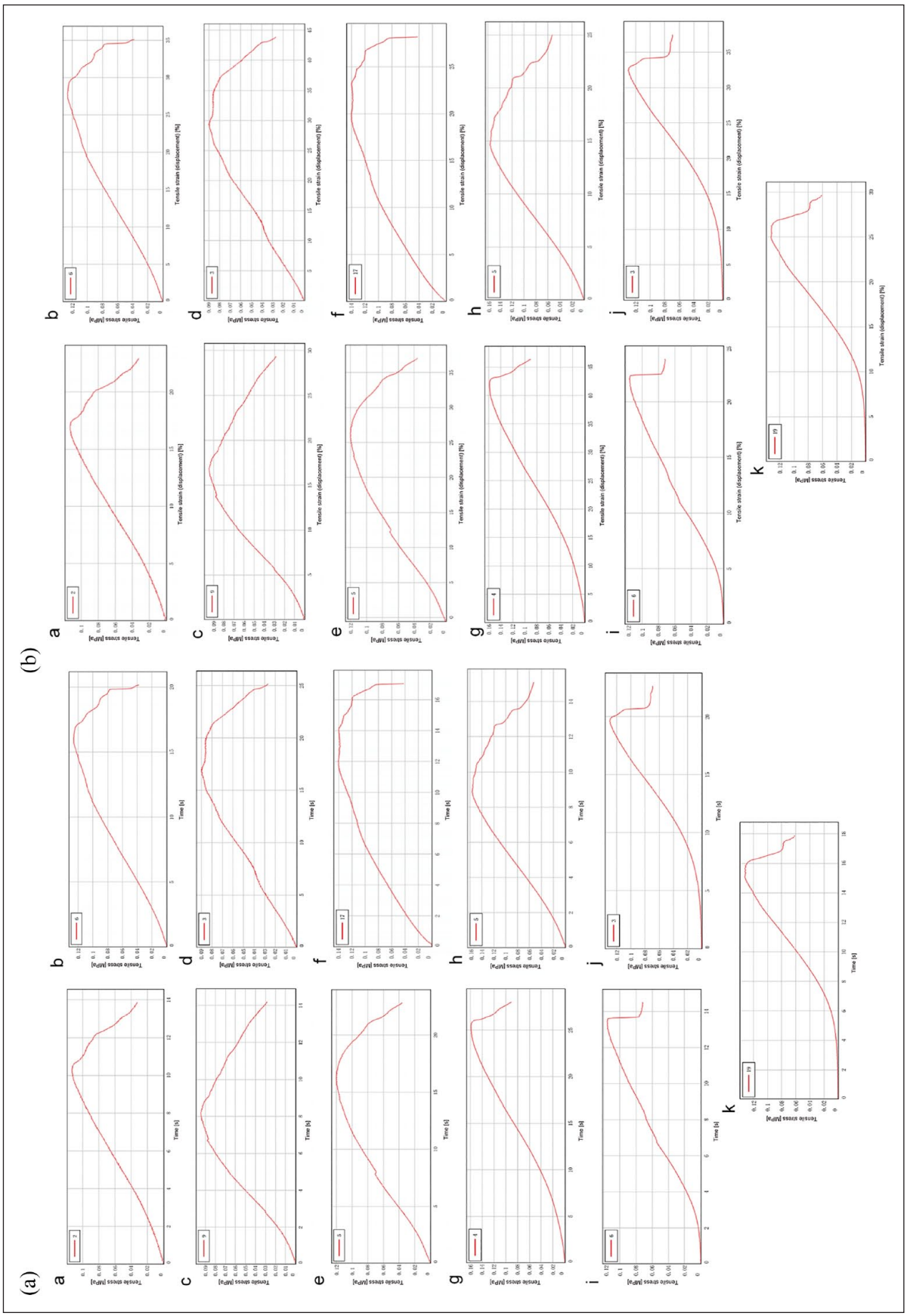

Figure 7. Stress-time curves (a) and stress-strain curves (b): (b-a)—(b-k) were control group, PGAM1, COL5A1, ANG, shRNH1, PGAM1/ANG, COL5A1/ANG, PGAM1/COL5A1, PGAM1/shRNH1, COL5A1/shRNH1, and ANG/shRNH1, respectively.

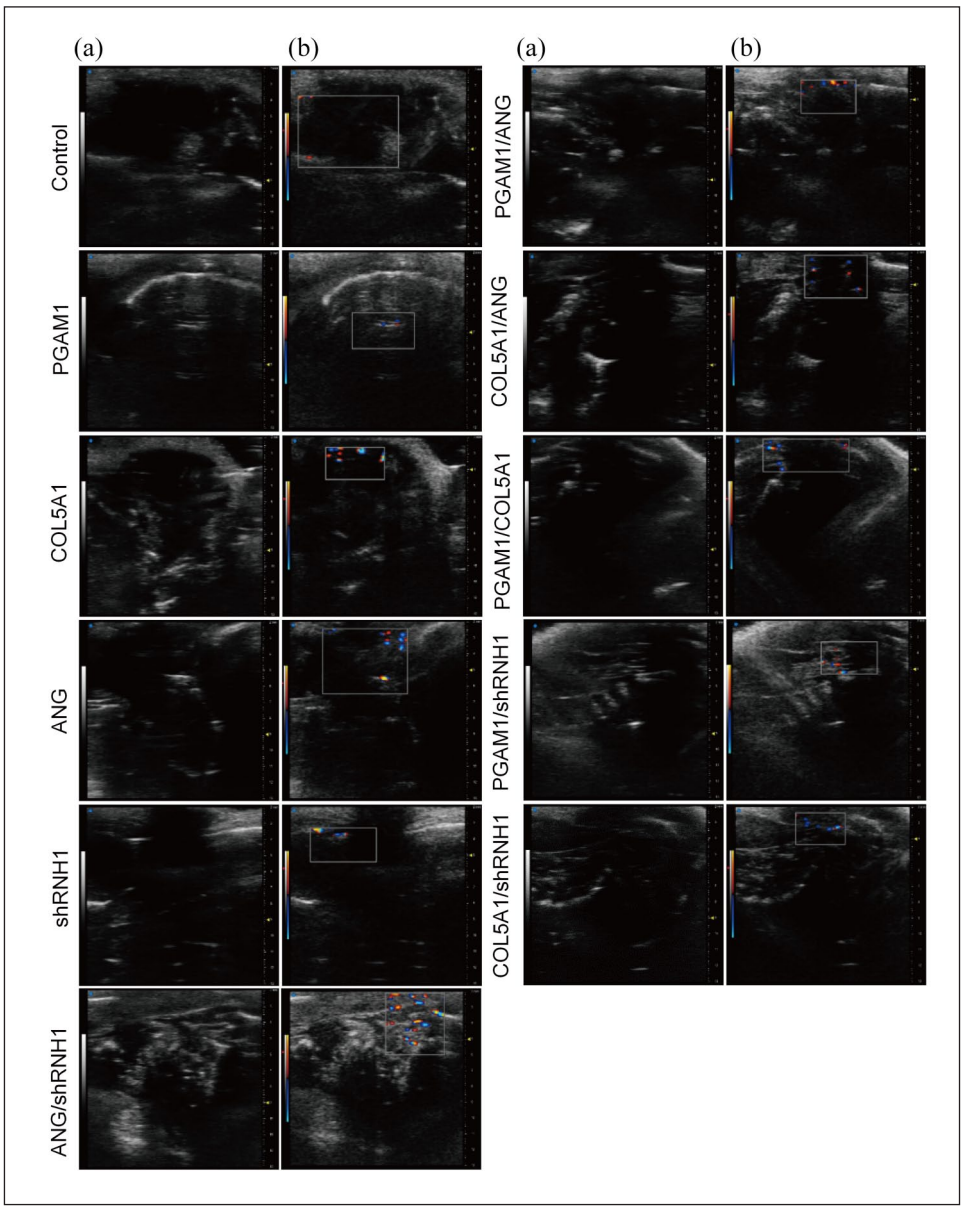

Figure 8. Analysis of vascularized blood flow signals of oral mucosal equivalents by small animals ultrasound: (a) gray-scale model was used to locate the equivalent vessel-like structure of oral mucosa, (b) the blood flow of the oral mucosal equivalent was observed by color doppler mode. Red represents flow toward the probe and blue represents flow away from the probe.

VELCs, especially the ANG/shRNH1 group. In addition, the number of branching points, total branching length, and total tubule length of the ANG/shRNH1 group were also increased compared with other groups. However, in vitro culture cannot fully simulate the in vivo environment, especially the information transmission between cells, which in turn affects the function of cells and tissues.[33] Bioreactor is an in vivo construction method to realize the vascularization of tissue engineering, which can simulate the human environment, provide suitable growth conditions for cells or tissues, and cultivate three-dimensional cells or tissues with similar structure and function as in vivo.[34] Based on this, we performed vascularization characterization and functional regeneration monitoring of the modified VOME in vivo. The results showed that the vessel-like structures anastomosed with the blood vessels in the bioreactor to form a vascular network and establish good blood circulation in the ANG/shRNH1 group. There were multi-directional vascular signals in all groups, but the ANG/shRNH1 group had the most significant blood flow signal. The growth and maturation of neovascularization are complex and coordinated processes that depend on the dynamic balance between angiogenic promoters and inhibitors.[35] ANG is a member of the ribonuclease (RNase) superfamily,[36] and RNH1 is an inhibitor of RNase. RNH1 has a high affinity for ANG and can bind and inhibit the

biological activity of ANG at a ratio of 1:1.[37] The reverse interaction between them showed that they promoted angiogenesis to achieve homeostatic vascularization and functional regeneration of oral mucosal equivalents.

The oral cavity is continuously subjected to soft tissue mechanical transduction[38]; therefore, the equivalent implanted at the damaged oral mucosa should have favorable mechanical properties to withstand normal oral chewing activities and ensure that no deformation or rupture occurs after implantation. Since previous study has compared the tensile stress of the native oral mucosa (0.048 ± 0.003 MPa) and the VOME (0.045 ± 0.002 MPa),[6] this study further compared VOME and its modified group. The results showed that the tensile stress of the modified VOME groups was higher than that of the VOME (0.11 ± 0.01 MPa). Although there was no significant difference in the maximum tensile stress among the groups, the tensile strain of the COL5A1/ANG group was higher than other groups when the maximum tensile stress was reached, and the difference was statistically significant, suggesting that the COL5A1/ANG modified oral mucosal equivalent had good biological properties. Combined with SEM, the vascular-like structure of the oral mucosa equivalent in the COL5A1/ANG group was observed to anastomose with the blood vessels of the bioreactor to form a vascular network, forming a chimera composed of the equivalent and the blood vessels of the bioreactor, which may provide a strong condition for the mechanical properties of the oral mucosa equivalent. COL5A1, as a collagen protein, can encode the proα1 chain of type V collagen, a major regulator of collagen fibril formation, which is required for skin integrity.[39] ANG can promote angiogenesis and indirectly stimulate the formation of collagen fibers by activating the entry of fibroblasts and their cytokines.[40] Therefore, high expression of COL5A1 and ANG may improve the mechanical properties of VOME.

Conclusion

In summary, this study confirmed that VHPOME based on the 3D cell technologies can achieve favorable vascularization. COL5A1/ANG may improve the mechanical properties of oral mucosal equivalents. The ANG-RNH1 system may play a significant role in establishing vascularization homeostasis and functional regeneration of oral mucosa equivalents, and future studies will further reveal the underlying mechanisms.

Acknowledgements

Not applicable.

Authors' contributions

Xuqian Liu conceived and designed the study. Xuqian Liu and Shigang Yin contributed the materials. Lijuan Shi, Yiwen Xu, Jingying Li and Li He performed the experiment and acquired data. Xuqian Liu, Lijuan Shi and Kaiyu Li analyzed and interpreted the data. Xuqian Liu, Lijuan Shi and Minhai Nie contributed significantly in writing the manuscript. All authors read and approved the final manuscript.

Data availability statement

Data will be made available on request.

Declaration of conflicting interests

The author(s) declared no potential conflicts of interest with respect to the research, authorship, and/or publication of this article.

Funding

The author(s) disclosed receipt of the following financial support for the research, authorship, and/or publication of this article: This work was supported by National Natural Science Foundation of China (82401112), the Open Project of National Key Laboratory of Oral Disease Prevention and Treatment (SKLOD2024OF04), and the Science and Technology Innovation Talent Program of Luzhou Science and Technology Knowledge Bureau (2023RCX171).

Ethics approval statement

This study has been approved by the Ethics Committee of Biomedical Scientific Research, Affiliated Stomatological Hospital of Southwest Medical University (No. 201909-1, No. 20190828001).

Informed consent statement

Informed consent was obtained from all patients for being included in the study.

ORCID iD

Xuqian Liu https://orcid.org/0000-0001-5646-5606

Supplemental material

Supplemental material for this article is available online.

References

1. Luo R, Fan Y, Liu H, et al. Application of tissue engineering scaffolds in the reconstruction of oral and maxillofacial soft tissue defects. *J Med Res* 2023; 52: 18–22.
2. Izumi K, Yortchan W, Aizawa Y, et al. Recent trends and perspectives in reconstruction and regeneration of intra/extra-oral wounds using tissue-engineered oral mucosa equivalents. *Jpn Dent Sci Rev* 2023; 59: 365–374.
3. Vargas-Valderrama A, Messina A, Mitjavila-Garcia MT, et al. The endothelium, a key actor in organ development and hPSC-derived organoid vascularization. *J Biomed Sci* 2020; 27: 67.
4. Shen J, Ouyang Z, Zhong J, et al. Research progress on vascularization of organoids. *Sheng wu yi xue gong cheng xue za zhi = J Biomed Eng = Shengwu yixue gongchengxue zazhi* 2023; 40: 625–631.
5. Qiu YL, Chen X, Hou YL, et al. Characterization of different biodegradable scaffolds in tissue engineering. *Mol Med Rep* 2019; 19: 4043–4056.

6. Liu X, Wang J, Dong F, et al. Study of composite vascular scaffold combining with differentiated VSMC- and VEC-like cells in vitro and in vivo. *J Biomater Appl* 2017; 32: 219–229.
7. Masson-Meyers DS, Bertassoni LE and Tayebi L. Oral mucosa equivalents, prevascularization approaches, and potential applications. *Connect Tissue Res* 2022; 63: 514–529.
8. Heller M, Frerick-Ochs EV, Bauer HK, et al. Tissue engineered pre-vascularized buccal mucosa equivalents utilizing a primary triculture of epithelial cells, endothelial cells and fibroblasts. *Biomaterials* 2016; 77: 207–215.
9. Cui X, Li Z and Yuan Y. Knockdown of FOXO4 protects against OGD/R-induced cerebral microvascular endothelial cell injury and regulates the AMPK/Nrf2/HO-1 pathway through transcriptional activation of CTRP6. *Exp Ther Med* 2024; 27: 94.
10. Estridge RC, O'Neill JE and Keung AJ. Matrigel tunes H9 stem cell-derived human cerebral organoid development. *Organoids* 2023; 2: 165–176.
11. Zhou M, Chen X, Qiu Y, et al. Study of tissue engineered vascularised oral mucosa-like structures based on ACVM-0.25% HLC-I scaffold in vitro and in vivo. *Artif Cells Nanomed Biotechnol* 2020; 48: 1167–1177.
12. Van Pham P, Vu NB, Dao TT, et al. Production of endothelial progenitor cells from skin fibroblasts by direct reprogramming for clinical usages. *In Vitro Cell Dev Biol Anim* 2017; 53: 207–216.
13. Zheng Y and Lu Y. Application of laser capture microdissection in the study of skin diseases. *China J Lepr Skin Dis* 2022; 38: 132–134.
14. Zhang L, Zhang Y, Zhou J, et al. Combined transcriptome and proteome analysis of yak PASMCs under hypoxic and normoxic conditions. *PeerJ* 2022; 10: e14369.
15. De Bock K, Georgiadou M, Schoors S, et al. Role of PFKFB3-driven glycolysis in vessel sprouting. *Cell* 2013; 154: 651–663.
16. Wang H, Yang M, Wang R, et al. On advance in the application of collagen to vascular grafts. *Chin Pharm Aff* 2022; 36: 836–842.
17. Tavernier Q, Bennana E, Poindessous V, et al. Regulation of IRE1 RNase activity by the Ribonuclease inhibitor 1 (RNH1). *Cell Cycle* 2018; 17: 1901–1916.
18. Bombaci G, Sarangdhar MA, Andina N, et al. LRR-protein RNH1 dampens the inflammasome activation and is associated with COVID-19 severity. *Life Sci Alliance* 2022; 5: e202101226.
19. Mueller T, Freystein J, Lucas H, et al. Efficacy of a bispecific antibody co-targeting VEGFA and Ang-2 in combination with chemotherapy in a chemoresistant colorectal carcinoma xenograft model. *Molecules (Basel, Switzerland)* 2019; 24: 2865.
20. Guo Y, Mei F, Huang Y, et al. Matrix stiffness modulates tip cell formation through the p-PXN-Rac1-YAP signaling axis. *Bioact Mater* 2022; 7: 364–376.
21. Weng C, Dong H, Mao J, et al. Characterization and function of the interaction of angiogenin with alpha-actinin 2. *Front Mol Biosci* 2022; 9: 837971.
22. Caligiuri G. CD31 as a therapeutic target in atherosclerosis. *Circ Res* 2020; 126: 1178–1189.
23. Noguchi Y, Maeda A, Wang HT, et al. Human CD31 on swine endothelial cells induces SHP-1 phosphorylation in macrophages. *Transplant Proc* 2020; 52: 1913–1915.
24. Sahoo S, Klychko E, Thorne T, et al. Exosomes from human CD34(+) stem cells mediate their proangiogenic paracrine activity. *Circ Res* 2011; 109: 724–728.
25. Caligiuri G. Mechanotransduction, immunoregulation, and metabolic functions of CD31 in cardiovascular pathophysiology. *Cardiovasc Res* 2019; 115: 1425–1434.
26. Mathiyalagan P, Liang Y, Kim D, et al. Angiogenic mechanisms of human CD34(+) stem cell exosomes in the repair of ischemic hindlimb. *Circ Res* 2017; 120: 1466–1476.
27. Wu H, Yin G, Pu X, et al. Inhibitory effects of combined bone morphogenetic protein 2, vascular endothelial growth factor, and basic fibroblast growth factor on osteoclast differentiation and activity. *Tissue Eng Part A* 2021; 27: 1387–1398.
28. Yang M, Li CJ, Xiao Y, et al. Ophiopogonin D promotes bone regeneration by stimulating CD31(hi) EMCN(hi) vessel formation. *Cell Prolif* 2020; 53: e12784.
29. Naito H, Iba T and Takakura N. Mechanisms of new blood-vessel formation and proliferative heterogeneity of endothelial cells. *Int Immunol* 2020; 32: 295–305.
30. Wang C, Dai X, Wu S, et al. FUNDC1-dependent mitochondria-associated endoplasmic reticulum membranes are involved in angiogenesis and neoangiogenesis. *Nat Commun* 2021; 12: 2616.
31. Modena DAO, Soares CD, Candido EC, et al. Effect of extracorporeal shock waves on inflammation and angiogenesis of integumentary tissue in obese individuals: stimulating repair and regeneration. *Lasers Med Sci* 2022; 37: 1289–1297.
32. Caldas P, Luz M, Baseggio S, et al. Transcription readthrough is prevalent in healthy human tissues and associated with inherent genomic features. *Commun Biol* 2024; 7: 100.
33. Broekman ML, Maas SLN, Abels ER, et al. Multidimensional communication in the microenvirons of glioblastoma. *Nat Rev Neurol* 2018; 14: 482–495.
34. Mahfouzi SH, Amoabediny G and Safiabadi Tali SH. Advances in bioreactors for lung bioengineering: from scalable cell culture to tissue growth monitoring. *Biotechnol Bioeng* 2021; 118: 2142–2167.
35. Cucci LM, Satriano C, Marzo T, et al. Angiogenin and copper crossing in wound healing. *Int J Mol Sci* 2021; 22: 10704.
36. Huang X, Liu F, Li Y, et al. Angiopoietins and female reproduction. *Acta Medicinae Universitatis Scientiae et Technologiae Huazhong* 2019; 48: 619–622.
37. Sarangdhar MA and Angiogenin AR. (ANG)-Ribonuclease inhibitor (RNH1) system in protein synthesis and disease. *Int J Mol Sci* 2021; 22: 1287.
38. Li Y, Zhang J, Cai W, et al. CREB3L2 regulates hemidesmosome formation during epithelial sealing. *J Dent Res* 2023; 102: 1199–1209.
39. Kiener S, Apostolopoulos N, Schissler J, et al. Independent COL5A1 variants in cats with Ehlers-Danlos syndrome. *Genes* 2022; 13: 797.
40. Yurina NV, Ageeva TA, Goryachkin AM, et al. Effects of recombinant angiogenin on collagen fiber formation and angiogenesis in the dermis of wistar rats. *Clin Cosmet Investig Dermatol* 2021; 14: 187–196.